Analysis of Microstructural Changes in the Heat-Affected Zone and Fusion Zone of a Fiber Laser Welded DP980 Steel

JIANQI ZHANG, ABDUL KHAN, OLANREWAJU A. OJO, NORMAN ZHOU, and DAOLUN CHEN

Dual phase (DP) steels are designed to consist of hard martensite dispersed in a relatively soft ferrite matrix, which offers a favorable combination of high strength with good deformability. Fiber laser welding (FLW) is becoming increasingly important for joining advanced materials due to its flexibility and deep penetration. In this study, the microstructure of a DP steel, DP980, welded by FLW technique was carefully analyzed. Gleeble thermo-mechanical simulation coupled with analytical transmission electron microscopy revealed that the FLW process produced significant microstructural changes in a narrow heat-affected zone (HAZ) and fusion zone (FZ), which can result in dramatic changes in mechanical properties. This is reflected in the micro-hardness profile obtained across the welded material. The salient phase transitions induced by the FLW, including the formation of new martensite grains in the upper-critical HAZ and FZ, are discussed.

DOI: 10.1007/s11663-014-0283-9

I. INTRODUCTION

In the automotive industry, dual phase (DP) steels are quickly becoming one of the most popular materials for structural applications in light weight vehicles.[1] The term 'dual phase' indicates that the steel has two distinct phases, *i.e.*, martensite and ferrite. Martensite is a very hard phase with body-centered tetragonal structure, while ferrite is a relatively soft phase with a body-centered crystal structure. Therefore, DP steels possess high strength and good ductility properties,[2,3] which enable automakers to produce vehicles with improved fuel economy and safety.

Welding is a technique widely used in the automotive industry. Despite the fact that laser welding cannot be used on reflective materials, it is still an enabling technology that is versatile, easy to use, and precise. Recently, fiber laser welding (FLW) has been developed and receiving attention due to its multiple advantages such as low maintenance costs and high efficiency, and produces deep penetration at high-welding speed.[4–6]

The use of DP steels for automotive structural applications is an effective way to reduce weight while improving the performance of vehicles. The welding of DP steels is an essential procedure during manufacturing. However, one issue in the application of welded DP steels is that the rapid thermal cycle involved in FLW can significantly change the mechanical properties of the welded materials, especially high strength grade steels such as DP980.[7–9] The evaluation of microstructural changes induced by welding is, nonetheless, vital in order to understand and predict how FLW affects the mechanical properties of the welded materials. However, it is very difficult to properly elucidate microstructural changes that occur during welding as the FLW generates narrow welds that contain large microstructural gradients.

Only a few studies have systematically investigated the microstructural changes of fiber laser welded DP980 steel. Therefore, the objective of this study was to study and understand the microstructural changes in welded DP980 steel caused by FLW.

II. MATERIALS AND EXPERIMENTAL PROCEDURE

The thickness of the DP980 steel sheets is 1.2 mm. The detailed chemistry composition of DP980 steel is listed in Table I. An IPG Photonics YLR-6000 FLW machine operated at 6 kW was used, with a welding speed of 16 m/min, a beam spot size of 0.6 mm, and a focal length of 30 mm. Welding was performed perpendicular to the work pieces without shielding gases. Heat-affected zone (HAZ) microstructure simulation was conducted on a Gleeble 1500D thermo-mechanical weld simulator built by Dynamic Systems, Inc, with a heating rate of 200 °C/s, peak temperatures of 373 K to 1473 K (100 °C to 1200 °C), a 0.5 second holding time and then water quenched. Figure 1 shows real time–temperature plots of simulation.

Samples for microstructure characterization were prepared using standard methods. The solution used for etching was 2 pct Nital and for electropolishing was

JIANQI ZHANG, Former Graduate Student, ABDUL KHAN, Research Officer, and OLANREWAJU A. OJO, Professor, are with the Department of Mechanical Engineering, University of Manitoba, Winnipeg, MB R3T 2N2, Canada. Contact e-mail: olanrewaju.ojo@umanitoba.ca NORMAN ZHOU, Professor, is with the Department of Mechanical and Mechatronics Engineering, University of Waterloo, Waterloo, ON, Canada. DAOLUN CHEN, Professor, is with the Department of Mechanical and Aerospace Engineering, Ryerson University, 350 Victoria Street, Toronto, ON, Canada.

Manuscript submitted September 10, 2014.
Article published online January 7, 2015.

Table I. Main Chemical Composition (Weight Percent) of DP980 Steel

Element	C	Mn	P	S	Si	Cu	Ni	Cr
DP980	0.15	1.50	0.01	0.006	0.31	0.02	0.01	0.02

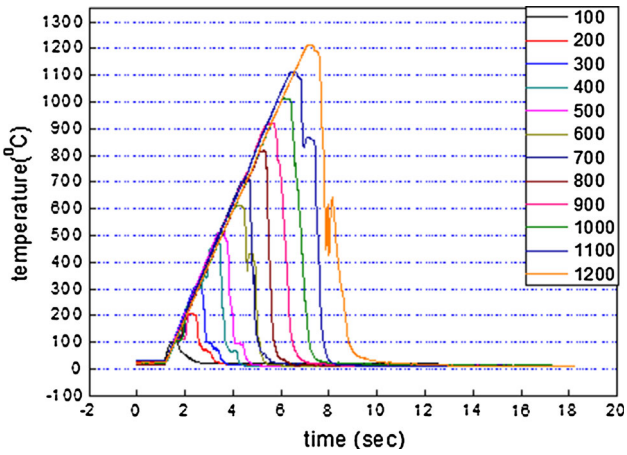

Fig. 1—Gleeble real time–temperature profile for the HAZ microstructure simulation.

a solution of 10 pct percholoric and 90 pct methanol. A microstructural analysis was carried out using an optical microscope (OM) (ZEISS Axiovert 25 inverted-reflected light microscope equipped with CLEMEX Vision 3.0 image analysis software), JEOL 5900 scanning electron microscope (SEM), and a JEOL 2000 FX transmission electron microscope (TEM). The microhardness profiles were obtained across the welded samples using a Buehler microhardness tester with a 200-g load and 15 seconds dwell time. The samples were etched to reveal the microstructure prior to testing. Sufficient space between indentations was ensured to avoid the strain effect of the adjacent indentations.

III. RESULTS AND DISCUSSION

A. *Microstructure Evolution*

Figures 2(a) and (b) show OM and SEM micrographs representing the typical microstructure of the DP980 steel. As reported by De *et al.*,[10] the ferrite appears bright while bainite and martensite appear dark under OM when the steel is etched by Nital solution. As shown in Figure 2(a), the bright phase is likely to be ferrite and dark phase is likely to be martensite or bainite. The volume fraction of the dark islands in the DP980 BM was estimated to be about 55 pct based on OM image

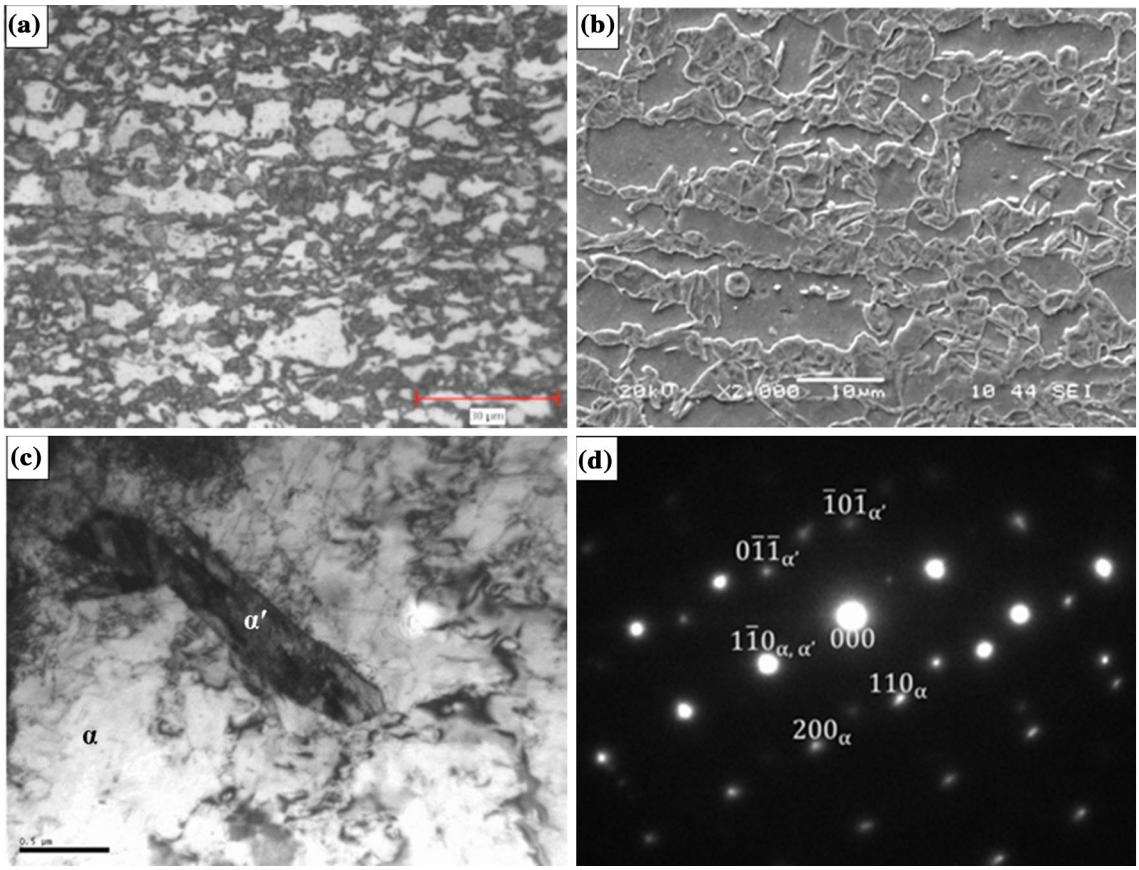

Fig. 2—(*a*) OM, (*b*) SEM, (*c*) BF micrographs of the DP980 steel, and (*d*) corresponding SADP of martensite and ferrite with the orientation of $[001]_{\alpha}//[\bar{1}\bar{1}1]_{\alpha' prime}$.

analysis. A higher magnification SEM micrograph (Figure 2(b)) shows a continuous matrix with patches of islands. The islands are likely to be martensite while the matrix is likely to be ferrite.[2,7–9,11–14] TEM was used to confirm the phases in the DP980 steel. A TEM bright field (BF) image of the DP980 steel is shown in Figure 2(c), and selected area diffraction pattern (SADP) analysis (Figure 2(d)) confirmed that the matrix is ferrite and the islands are martensite. The orientation relationship between ferrite and martensite is $[001]_{Ferrite}//[\bar{1}\bar{1}1]_{Martensite}$.

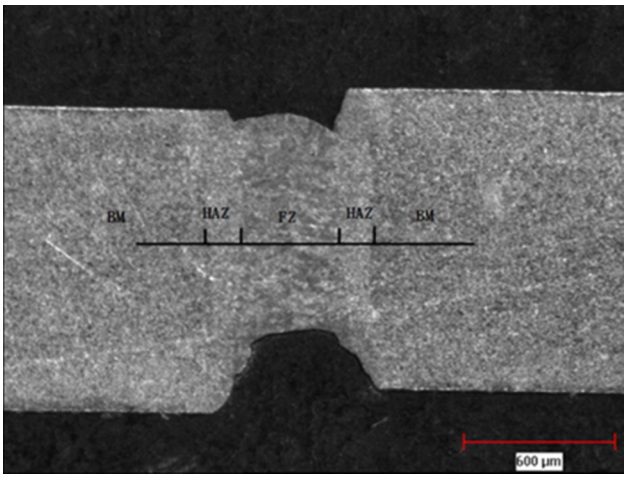

Fig. 3—An overview of fiber laser welded steel.

By analyzing the microstructure of the cross section of fiber laser welded steels, three different regions are found as shown in Figure 3. The fusion zone (FZ) is in the middle, with adjacent HAZs and followed by unaffected BM on each side. The widths of the FZ and HAZ are about 400 to 500 and 150 to 250 μm, respectively. Xia *et al.*[15] reported that the diode laser welding of DP980 steel with a laser power of 4 kW resulted in 4 and 3 mm wide HAZ and FZ, respectively. The narrower HAZ and FZ widths in the present work are due to higher energy density and smaller beam size of FLW compared with that of diode laser welding.[7] In addition, higher welding speed can lead to a narrower weld.[9]

Figure 4 shows SEM micrograph of a typical microstructure of the HAZ in the DP980 steel. The HAZ can be divided into three regions, *i.e.*, HAZ-1, HAZ-2, and HAZ-3 as labeled in image. In the HAZ-1, the martensite presented in the alloy prior to weld appears to have decomposed. In the HAZ-2, it appears that a new microconstituent which increases with increasing proximity to HAZ-3 was formed. In HAZ-3, the newly formed microconstituent becomes the dominant feature. The newly formed microconstituent appears to have martensitic or bainitic structure based on the SEM examination. The microstructural analysis of simulated samples found that when the simulation temperature is

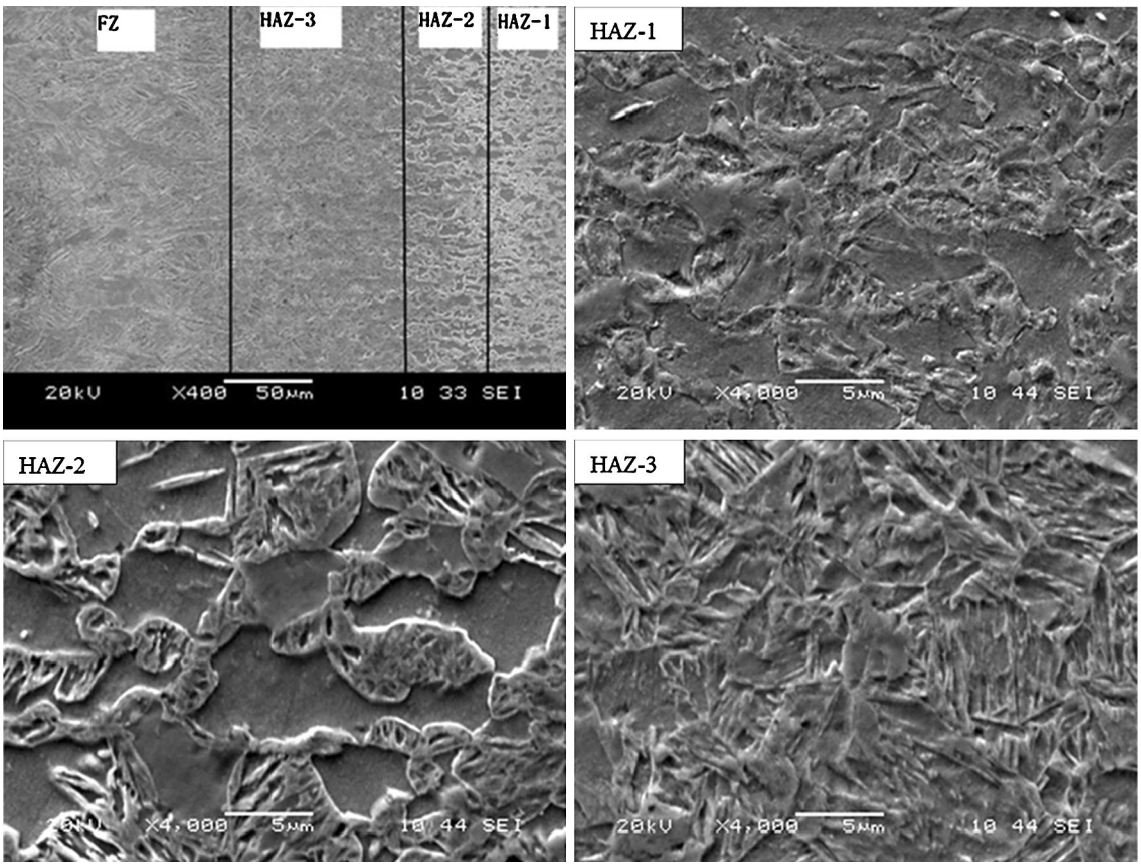

Fig. 4—Micrographs of the HAZ in laser welded DP980 steel.

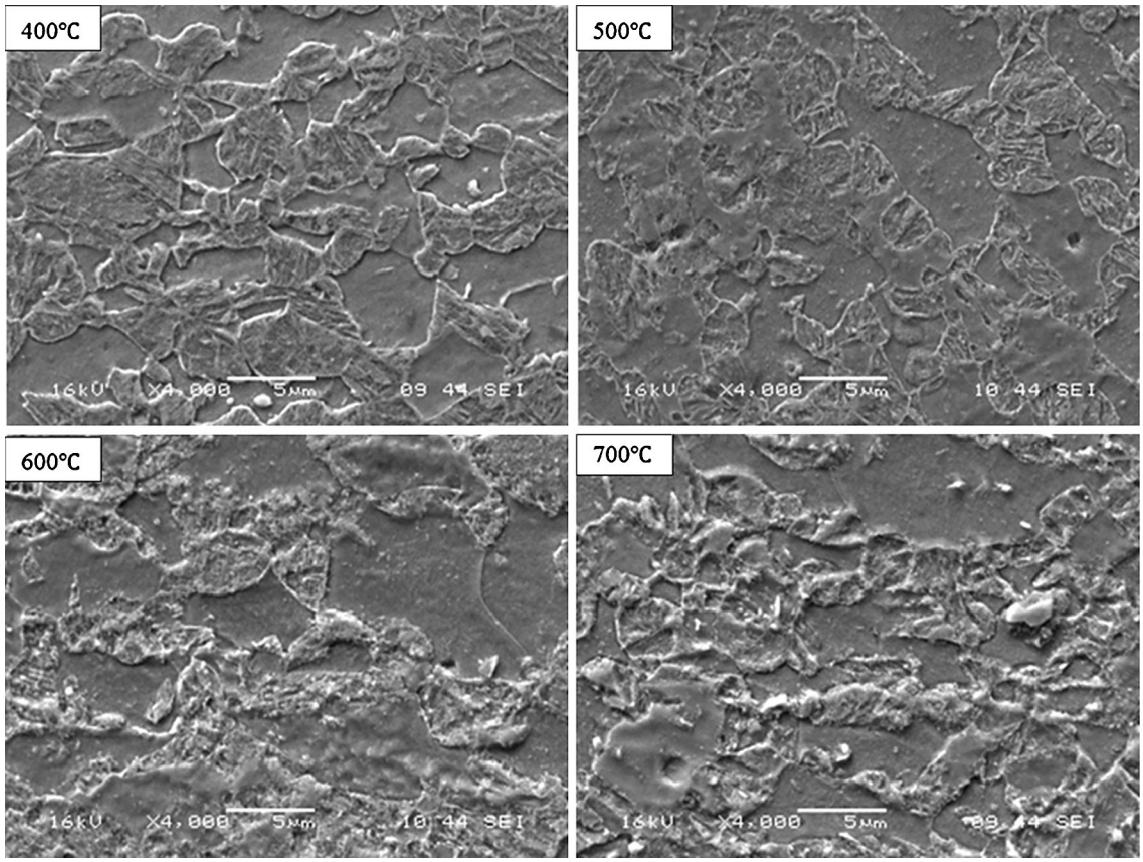

Fig. 5—SEM micrographs of the Gleeble simulated HAZ of the DP980 steel with peak temperatures of 673 K to 973 K (400 °C to 700 °C).

lower than 573 K (300 °C), no significant microstructure changes is discernable by the use of the SEM.

At the simulation temperature range of 673 K to 973 K (400 °C to 700 °C), the microstructure of simulated samples is similar to the actual weld HAZ-1. Figure 5 shows the SEM micrograph of sample simulated at 673 K to 973 K (400 °C to 700 °C). It appears that some fine particles were formed within the martensite at 673 K and 773 K (400 °C and 500 °C). At temperatures of 873 K and 973 K (600 °C and 700 °C), the decomposition of martensite and fine particles become more obvious. The fine particles are likely carbides formed due to the tempering of martensite at this temperature range.

At the simulation temperature range of 1073 K to 1173 K (800 °C to 900 °C), the microstructure of simulated samples is similar to the HAZ-2. Figure 6 shows the SEM micrograph of sample simulated at 1073 K to 1473 K (800 °C to 1200 °C). The microstructure suggests that no martensite tempering occurred at these temperatures, and possible new martensite grains were formed. At 1173 K (900 °C), an almost fully martensitic or bainitic structure was formed. Above 1173 K (900 °C), the microstructure of simulated samples is similar to the HAZ-3 of welded sample. The SEM micrographs of simulated samples at the temperature range of 1173 K to 1473 K (900 °C to 1200 °C) are shown in Figure 6. It can be observed that fully martensitic or bainitic structure is formed at temperatures above 1173 K (900 °C), and an increase of the packet size of the microstructure can also be observed as temperature increased. The lath-like structure of simulated samples at this temperature range is similar to the microstructure of the region very close to the FZ of the welded sample.

TEM was then carried out to further study the microstructures in the HAZ of DP980 steel. The typical peak temperatures chosen for HAZ-1 and HAZ-3 studies are 923 K and 1273 K (650 °C and 1000 °C), respectively. Figure 7(a) is a BF image that shows some particles dispersed in the matrix of simulated HAZ-1 sample. TEM SADP analysis showed the particles to be cementite and the matrix to be ferrite with an orientation relationship of $[\bar{1}\bar{1}0]$cementite//$[\bar{2}00]$ferrite (Figure 7(c)). A corresponding dark field (DF) image taken using the $g = \bar{1}10$ cementite reflection revealed the cementite particles as shown in Figure 7(b).

Figure 8(a) shows a BF image of lath microstructure of the simulated HAZ-3 sample. TEM SADP analysis confirmed that the structure consists of lath martensite and interlath austenite. The corresponding DF image taken using the $g = 200$ austenite reflection (label as A) revealed the interlath austenite as shown in Figure 8(c). Twinned martensite was also occasionally observed. The corresponding DF image taken using the circled twinned martensite reflection in the inserted SADP revealed twinned martensite as shown in Figure 8(b). As previously stated, the HAZ of the welded DP980 steel can be divided into three regions: HAZ-1, HAZ-2, and HAZ-3. In the HAZ-1, the steel experienced thermal cycles to

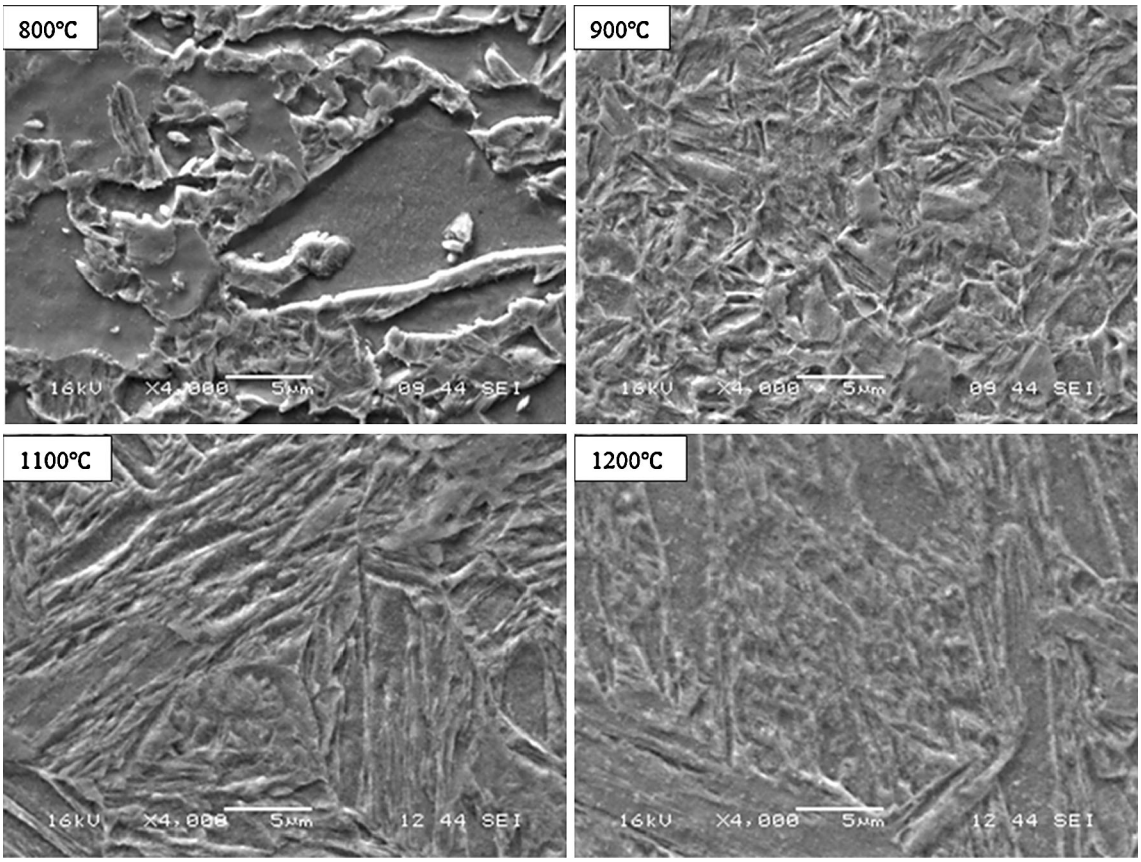

Fig. 6—SEM micrographs of the Gleeble simulated HAZ of the DP980 steel with peak temperatures of 1073 K to 1473 K (800 °C to 1200 °C).

peak temperatures from about 673 K to 973 K (400 °C to 700 °C). At these temperatures, the martensite was decomposed into cementite particles dispersed within the ferrite matrix. Since the Gleeble simulation study in this work showed that the phases are formed within the temperature range of 673 K to 973 K (400 °C to 700 °C), therefore HAZ-1 is sub-critical HAZ section. Previous research also found tempered martensite in the sub-critical HAZ of welded DP steels.[16–18]

In the HAZ-2, the steel experienced thermal cycles to peak temperatures from 1073 K to 1173 K (800 °C to 900 °C). New martensite formed in this region, and the newly formed martensite increases in amount with increasing proximity to the HAZ-3. Since the Gleeble simulation study in this work showed that the phases are formed within the temperature range of 1073 K to 1173 K (800 °C to 900 °C), therefore the HAZ-2 is the inter-critical HAZ region. In inter-critical HAZ, the steel was partially austenized during the heating process due to the thermal cycles involved during welding, and the austenite transformed to martensite upon rapid cooling.

In the HAZ-3, the steel experienced thermal cycles to peak temperatures above 1173 K (900 °C). The dominant phase found in the HAZ-3 is lath martensite phase, with thin retained austenite located in the interlath region. Since the Gleeble simulation study in this work showed that the phases are formed above 1173 K (900 °C), the HAZ-3 is upper-critical HAZ region, where the steel was fully austenized during the heating process. When the austenite rapidly cooled down, carbon atoms were trapped in the phase causing it to transform to martensite.[19]

The microstructure in the HAZ of fiber laser welded DP980 steel is significantly different from that in the BM. In the BM, the microstructure is relatively uniform, while there is a large microstructural gradient in the HAZ of the DP980 steel. Besides, in the BM, martensite and ferrite are the dominant phases, while the main phases in the sub-critical HAZ are ferrite and tempered martensite (ferrite and cementite), and in the upper-critical HAZ, the dominant phases are martensite and austenite. The changes in the microstructure in the HAZ of welded DP980 steel could significantly affect the mechanical properties of the DP980 steel. Previous studies[20,21] have showed that mechanical properties degradation occurred due to the martensite tempering in the subcritical HAZ of welded DP steel.

Figure 9(a) shows the SEM micrograph of the microstructure of the FZ of the DP980 steel. It appears from the microstructure that the FZ of DP980 steel has a fine martensitic or bainitic structure. Figure 9(b) shows a BF image of the FZ in DP980 steel, which reveals a lath microstructure. TEM SADP analysis confirmed the lath phase to be martensite and austenite as the interlath phases. SADP taken from [001] zone axis of martensite is shown in Figure 9(d), which indicates an orientation relationship of $[001]'_{\alpha}//[011]_{\gamma}$. DF image taken with $g = bar200$ austenite reflection is shown in Figure 9(c).

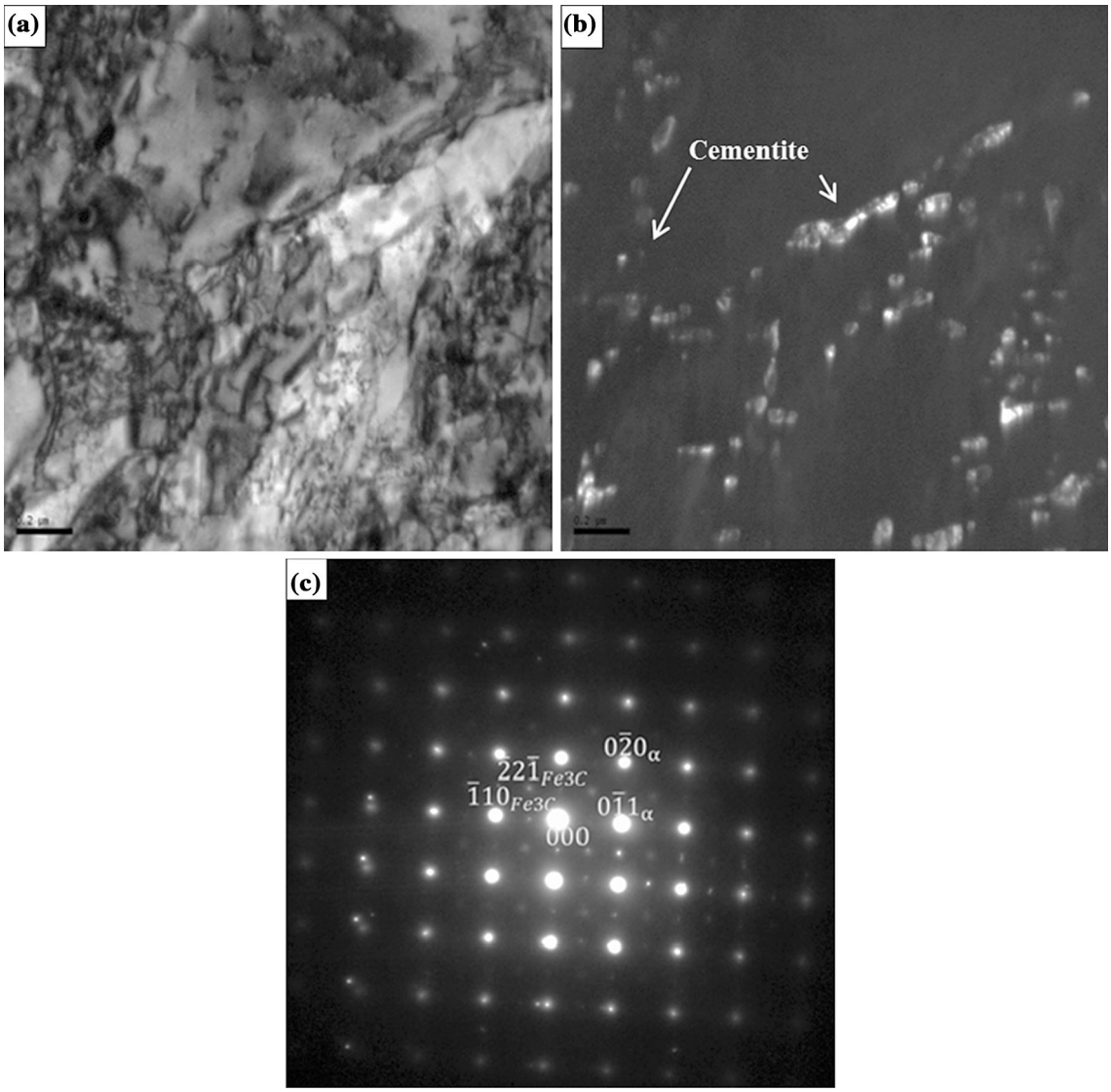

Fig. 7—(*a*) BF, (*b*) DF micrographs of simulated HAZ-1 of the DP980 steel, (*c*) Corresponding SADP of the cementite and ferrite.

The microstructure of the FZ is significantly different from that of the BM. Phases in the BM of the DP980 steel are mainly ferrite and martensite, while phases in the FZ of the DP980 steel are mainly martensite and austenite. The volume fraction of martensite in the BM is about 55 pct, while in the FZ more than 90 pct martensite is formed. The morphology of martensite in the FZ of the DP980 steel is ultra-fine lath, while the morphology of the martensite in the BM is island. The large difference in the microstructure between the FZ and the BM could result in dramatic changes in mechanical properties. The effect of microstructural changes due to welding on the microhardness of the steel will be further discussed into details in the Section III–B.

B. *Hardness*

Vickers microhardness profile across the welds of the fiber laser welded DP980 steel is measured and plotted in Figure 10(a), and the average hardness value of the Gleeble simulated samples is plotted in Figure 10(b). The average microhardness value of the BM of the DP980 steel was about 350 HV. The microhardness curve in Figure 10(a) shows two softened zones in the sub-critical HAZ, where the average micro-hardness value dropped significantly from 350 HV (BM) to 280 HV. Gleeble simulated results showed that there was a negligible change in the hardness value when the tested peak temperatures were between 373 K and 573 K (100 °C and 300 °C). As the peak temperature increased from 573 K (300 °C) onwards, reduction of hardness is also observed in simulated samples. The hardness of the DP980 steel decreased and reached the minimum value of 225 HV at peak temperature of 973 K (700 °C). The reason for the softening of the steel in the sub-critical HAZ is that the martensite locally tempered at this region. Visible martensite tempering started at the peak temperature of 673 K (400 °C), and the decomposing process accelerated as the temperature

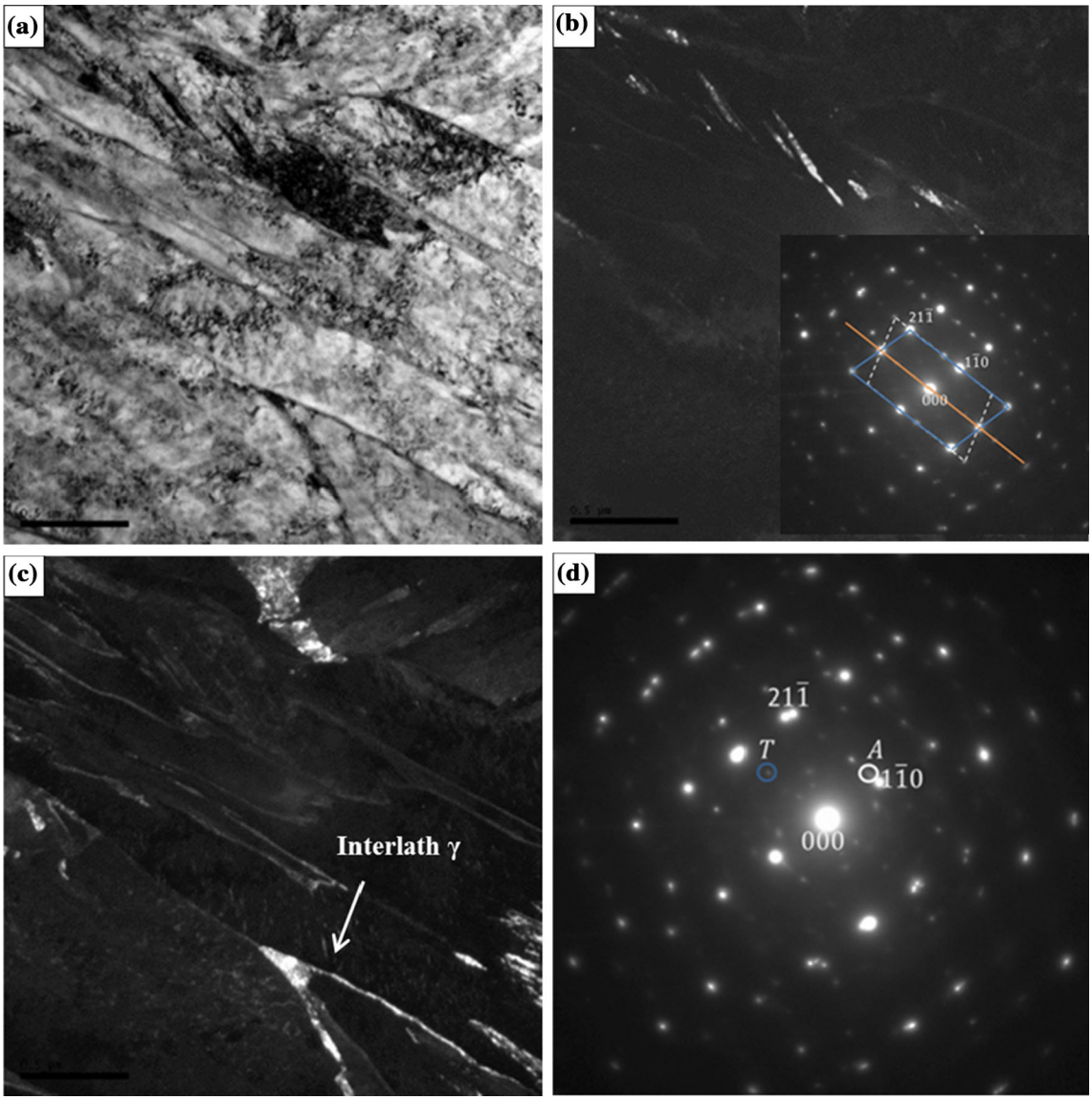

Fig. 8—(*a*) BF micrograph of simulated HAZ-3 of the DP980 steel, (*b*) DF micrograph with inset SADP showing twinned martensite, (*c*) DF micrograph using 200_{γ} spot showing interlath austenite, and (d) corresponding SADP from austenite (labeled as A), martensite, and twinned martensite.

increased until 973 K (700 °C). The tempering of martensite in the HAZ was responsible for the local weakening of the hardness in welded DP980 steels.

In the inter-critical HAZ, there is a sharp increase of the hardness, which is up to the hardness of FZ. Similar results were observed in the simulated samples at temperature range of 1073 K to 1173 K (800 °C to 900 °C). The hardness of simulated samples dramatically increased as the temperature increases from 1073 K (800 °C) to 1173 K (900 °C). This is because that in the inter-critical HAZ, the volume fraction of martensite increases with increasing proximity to the upper-critical HAZ. New martensite formed when the temperature reached 1073 K (800 °C), at which temperature the steel was partially austenitized. Increasing peak temperature results in more austenite formation, which in turn yields more martensite upon rapid cooling.

In the upper-critical HAZ, the hardness of the DP980 steel remains at high value which is equivalent to the hardness in the FZ. The hardness values of the simulated samples at a temperature range of 1173 K to 1473 K (900 °C to 1200 °C) are similar to those measured in the upper-critical HAZ of the welded DP980 steel. The hardness of simulated samples achieved almost a constant hardness value of 440 HV from the temperature of 1173 K (900 °C) until 1473 K (1200 °C). This is because when the temperature reached 1173 K (900 °C), almost full austenitization was achieved. The fast cooling rate induced by water quenching the sample at the peak temperature led to the formation of lath martensite.

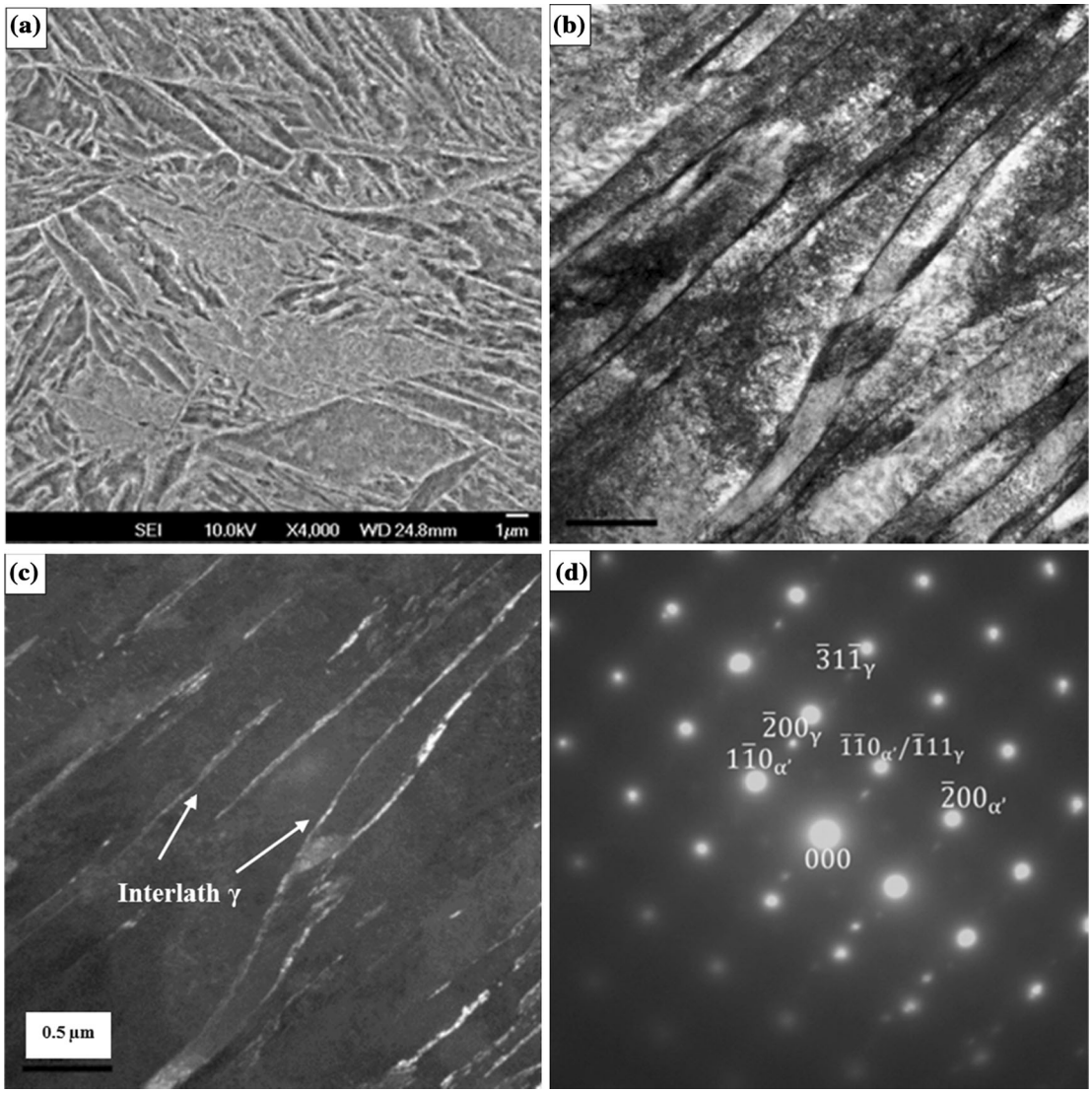

Fig. 9—(*a*) SEM, (*b*) BF micrographs of the FZ of the DP980 steel, (*c*) DF image taken using the $\bar{2}00$ austenite spot, and (*d*) corresponding SADP of austenite and martensite.

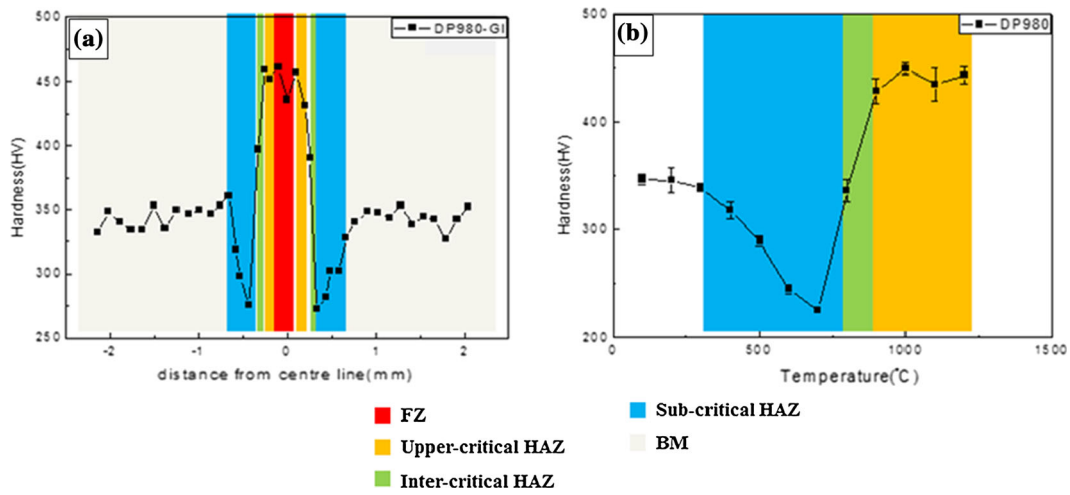

Fig. 10—(*a*) A microhardness profile of the fiber laser welded DP980 steel. (*b*) Microhardness of simulated DP980 steel.

IV. CONCLUSIONS

The microstructural changes that occurred in the HAZ and the FZ of a fiber laser welded DP980 steel were systematically studied by the use of Gleeble thermo-mechanical simulation system and TEM techniques. The following are the conclusions that can be drawn:

1. Fiber laser beam welding resulted in considerable microstructural changes in a narrow HAZ and FZ of the DP980 steel.
2. The analyses show that pre-weld martensite grains were severely tempered in the sub-critical HAZ, while extensive formation of new martensite occurred in the upper-critical HAZ and FZ.
3. The microstructural alteration in the HAZ and FZ resulted in notably disparate micro-hardness values in these regions compared with that of the BM.
4. Therefore, appropriate post-heat treatments may be required to modify the microstructure of the fiber laser welded DP980 steel in order to minimize variation in mechanical properties between the BM, HAZ, and FZ.

ACKNOWLEDGMENT

The authors gratefully acknowledge financial support for the project from the Auto21 Network of Centres of Excellence Program, Canada.

REFERENCES

1. R. Kuziak, R. Kawalla, and S. Waengler: *Arch. Civ. Mech. Eng.*, 2008, vol. 8, pp. 103–17.
2. J. Li, S.S. Nayak, E. Biro, S.K. Panda, F. Goodwin, and Y. Zhou: *Mater. Des.*, 2013, vol. 52, pp. 757–66.
3. M.P. Miles, J. Pew, T.W. Nelson, and M. Li: *Frict. Stir Weld. Process.*, 2005, vol. III, pp. 91–96.
4. C. Thomy, T. Seefeld, and F. Vollertsen: *Sheet Metal*, 2005, vol. 2005 (6–8), pp. 171–8.
5. F. Vollertsen: *Sheet Metal*, 2005, vol. 6-8, pp. 59–70.
6. G. Verhaeghe: *Weld. J.*, 2005, vol. 84, pp. 56–60.
7. N. Sreenivasan, M. Xia, S. Lawson, and Y. Zhou: *J. Eng. Mater. Technol.*, 2008, vol. 130, p. 041004.
8. W. Xu, D. Westerbaan, S.S. Nayak, D.L. Chen, F. Goodwin E. Biro, and Y. Zhou: *Mater. Sci. Eng. A*, 2012, vol. 553A, pp. 51–58.
9. W. Xu, D. Westerbaan, S.S. Nayak, D.L. Chen, F. Goodwin, and Y. Zhou: *Mater. Des.*, 2013, vol. 43, pp. 373–83.
10. A.K. De, J.G. Speer, and D.K. Matlock: *Adv. Mater. Process.*, 2003, vol. 161, pp. 27–30.
11. N. Farabi, D.L. Chen, and Y. Zhou: *J. Mater. Eng. Perform.*, 2011, vol. 21, pp. 222–30.
12. P.C. Seshagiri, G. Madhusudan Reddy, K. Srinivasa Rao, M. Govinda Raju, S.S. Bhattacharya, and K. Prasad Rao: *Sci. Technol. Weld. Join.*, 2008, vol. 13, pp. 415–21.
13. N. Farabi, D.L. Chen, and Y. Zhou: *J. Alloy. Compd.*, 2011, vol. 509, pp. 982–89.
14. D. Parkes, W. Xu, D. Westerbaan, S.S. Nayak, Y. Zhou, F. Goodwin, S. Bhole, and D.L. Chen: *Mater. Des.*, 2013, vol. 51, pp. 665–75.
15. M. Xia, N. Sreenivasan, S. Lawson, and Y. Zhou: *J. Eng. Mater. T*, 2007, vol. 129, pp. 446–52.
16. M.S. Xia, E. Biro, Z.L. Tian, and Y.N. Zhou: *ISIJ Int.*, 2008, vol. 48, pp. 809–14.
17. P.K. Ghosh: *ISIJ Int.*, 1990, vol. 30, pp. 317–24.
18. P.K. Ghosh, P.C. Gupta, R.A.M. Avtar, and B.K. Jha: *Weld. J.*, 1991, vol. 70, pp. S7–S14.
19. J.D. Verhoeven: *Steel Metallurgy for the Non-metallurgist*, ASM International, Materials Park, OH, 2007.
20. D.Y. Dong, Y. Liu, Y.L. Yang, J.F. Li, M. Ma, and T. Jiang: *Mater. Sci. Eng. A*, 2014, vol. 594, pp. 17–25.
21. S.S. Nayak, Y.Zhou, V.H.B. Hernandez, and E. Biro: *Trends in Welding Research: Proceedings of the 9th International Conference*, 2013, pp. 641–49.